0026-895X/03/6303-489–498$7.00
MOLECULAR PHARMACOLOGY
Vol. 63, No. 3
1989/1042362
Mol Pharmacol 63:489–498, 2003
Printed in U.S.A.

Influence of Molecular Structure on Substrate Binding to the Human Organic Cation Transporter, hOCT1

DALLAS BEDNARCZYK, SEAN EKINS,[1] JAMES H. WIKEL, and STEPHEN H. WRIGHT

Department of Physiology, University of Arizona, Tucson, Arizona (D.B., S.H.W.); and Computational Chemistry and Molecular Structure Research, Eli Lilly and Co., Indianapolis, Indiana (S.E., J.H.W.)

Received July 10, 2002; accepted November 4, 2002

This article is available online at http://molpharm.aspetjournals.org

ABSTRACT

Organic cation transporters play a critical role in the elimination of therapeutic compounds in the liver and the kidney. We used computational quantitative structure activity approaches to predict molecular features that influence interaction with the human ortholog of the organic cation transporter (hOCT1). [^{3}H]tetraethylammonium uptake in HeLa cells stably expressing hOCT1 was inhibited to varying extents by a diverse set of 30 molecules. A subset of 22 of these was used to produce, using Catalyst, a pharmacophore that consisted of three hydrophobic features and a positive ionizable feature. The correlation coefficient of observed versus predicted IC_{50} was 0.86 for this training set, which was superior to calculated logP alone (r = 0.73) as a predictor of hOCT1 inhibition. A descriptor-based quantitative structure-activity relationship study using Cerius^2 resulted in an equation relating five molecular descriptors to log IC_{50} with a correlation coefficient of 0.95. Furthermore, a group of phenylpyridinium and quinolinium compounds were used to investigate the spatial limitations of the hOCT1 binding site. The affinity for hOCT was higher for 4-phenylpyridiniums > 3-phenylpyridiniums > quinolinium, indicating that substrate affinity was influenced by the distribution of hydrophobic mass. In addition, supraplanar hydrophobic mass was found to increase the affinity for binding hOCT1. These results indicate how a combination of computational and in vitro approaches may yield insight into the binding affinity of transporters and may be applicable to predicting these properties for new therapeutics.

The transepithelial transport of organic cations (OCs) plays an important role in the excretion of xenobiotic compounds from the body by means of the liver and kidney, and from the cerebrospinal fluid via the choroid plexus (Pritchard and Miller, 1993). The proteins involved in the translocation of OCs transport a broad range of substrates. These substrates include naturally occurring plant alkaloids and synthetic drugs such as cimetidine and procainamide. These chemicals are not only therapeutically diverse but show remarkable structural diversity as well. A characterization of the structural parameters of substrates translocated by organic cation transporters may provide insight into the molecular determinants of substrate specificity (Ullrich, 1999). Because the elimination of many therapeutic drugs is significantly influenced by the interaction of these compounds with OC transporters, information pertinent to predicting the kinetics of such interactions may be useful in estimating the pharmacokinetics of a broad range of pharmaceuticals.

The organic cation transporter, OCT1, is likely to play a significant role in the elimination of a variety of therapeutic compounds. OCT1 is highly expressed in the sinusoidal membrane of liver cells (Meyer-Wentrup et al., 1998), where it is presumed to play a role in the hepatic metabolism and elimination of cationic drugs (Koepsell, 1998). In the rat, OCT1 is also expressed in the basolateral membrane of early (S1 segment) renal proximal tubule (Karbach et al., 2000), where it is presumed to play a role in the peritubular uptake step of OC secretion.

With the increasing number of discoveries of new molecules that interact with OC transporters (Zhang et al., 2000; Dresser et al., 2001), understanding the three-dimensional features fundamental to molecular interaction with the transporter is desirable. Hydrophobicity and basicity have been suggested to be the principal determinants of substrate interaction with OC transporters on both the apical and basolateral membranes of the rat renal proximal tubule (Ullrich et al., 1991). This observation was independently supported for apical and basolateral transporters in the rabbit (Groves et al., 1994; Wright et al., 1995; Wright and Wunz, 1999). However, the mechanisms of substrate interaction with proteins possessing multiple transmembrane domains are difficult to assess directly because of the absence of crys-

This work was supported in part by National Institutes of Health grants DK58251, ES06694, and HL07249.

[1] Present address: Concurrent Pharmaceuticals Inc., 502 West Office Center Drive, Fort Washington, PA 19034.

ABBREVIATIONS: OC, organic cation; OCT, organic cation transporter; 3D-QSAR, three-dimensional quantitative structure-activity relationship; TEA, tetraethylammonium; NBD-TMA, [2-(4-nitro-2,1,3-benzoxadiazol-7-yl)aminoethyl]trimethylammonium; PCR, polymerase chain reaction; nTAA, *n*-tetraalkylammonium; TBA, tetrabutylammonium; TPeA, tetrapentylammonium; TprA, tetrapropylammonium.

tal structures for these proteins. It is therefore desirable to take advantage of computational techniques such as three-dimensional quantitative structure-activity relationships (3D-QSAR) that may provide an effective means of assessing the basis of substrate-transporter interaction in the absence of knowledge of the 3D structure of the transport protein. Structure-activity relationships have been developed previously for substrates of the OC^+/H^+ exchanger (Wright and Wunz, 1999). Using this analysis, it was concluded that the binding site of the luminal transport step of rabbit renal proximal tubules, the OC^+/H^+ exchanger, includes a planar hydrophobic surface sufficiently accommodating that no steric exclusion is evident when a planar (9- × 12-Å) hydrophobic mass is rotated about an *N*-pyridinium center. This work, although comparatively rudimentary, introduced the use of structure-activity relationship analysis as a way to understand how therapeutics may interact with OC transporters.

In the present report, multiple QSAR approaches were used to assess the influence of selected structural and physical factors on substrate interaction with the human organic cation transporter, hOCT1. The first technique involved development of a computationally derived pharmacophore, a three-dimensional arrangement of important molecular features, based on the interaction of a structurally diverse set of OC inhibitors with hOCT1, complemented by a descriptor-based QSAR model that provided further insight into molecular interaction with the transporter. The descriptor-based computational analysis provided the basis for an empirical assessment of substrate-transporter interaction that used a strategically modified set of inhibitors to validate parameters identified in the descriptor-based analysis.

Materials and Methods

Materials. [^{3}H]Tetraethylammonium ([^{3}H]TEA; 13.2 Ci/mmol) was a custom synthesis by Amersham Biosciences (Piscataway, NJ). [^{3}H]1-Methyl-4-phenylpyridinium (80 Ci/mmol) was purchased from ARC, Inc. (St. Louis, MO). NBD-TMA was synthesized as described previously (Bednarczyk et al., 2000) (and is commercially available from Macrocyclics, Inc., TX). The phenylpyridinium and quinolinium analogs were synthesized as described previously (Wright et al., 1995). Other chemicals were purchased from Sigma Chemical Corp. (St. Louis, MO) or Aldrich Chemical Co. (Milwaukee, WI). Octanol/water partition coefficients (Log P) were calculated using CLOGP software (Daylight Chemical Information Systems; www.daylight.com).

Generation, Transfection, and Culture of HeLa Cells Expressing hOCT1 and hOCT1-V5His cDNAs. The hOCT1 cDNA in the pEXO vector was kindly provided by Dr. Kathleen M. Giacomini (University of California, San Francisco, CA). hOCT1 was removed from pEXO using *Kpn*I and *Xho*I and ligated into pIZ-V5His (Invitrogen, Carlsbad, CA). hOCT1 was removed from pIZ-V5His at *Hin*dIII and *Xho*I and ligated into pcDNA3.1 to generate a plasmid for production of wild-type hOCT1. Because of a future interest in isolating hOCT1 protein from cells, we generated a histidine-tagged hOCT1 sequence by muting the stop codon and introducing a frame shift mutation to interpose an alanine in frame with the V5His tag of the vector, pIZ-V5His. This was accomplished using the following primers: the OpIE2 promoter site on the plasmid was used as the forward primer (5′-CGCACCGATCTGGTAAACAC-3′) and 5′-GCCCTCTAGACTCGAGGCGGTGCCCGAGGGTTC-3′ as the reverse primer containing the mutated sequence. The mutated PCR fragment was cut at *Hin*dIII and *Xho*I to generate a full-length cDNA sequence that was ligated back into the parent vector. Another mutation was performed on the pIZ-hOCT1-V5His sequence to insert an *Eco*RI cut site after the stop codon of the His-tag using the reverse primer 5′-GGATTTAGTCAGATGAATTCAATGGTGATG-3′, in conjunction with the forward primer for the OpIE2 promoter priming site on the plasmid. The resulting PCR fragment was digested with *Hin*dIII and *Eco*RI and ligated into pUC18, from which it was digested with *Bam*HI and *Eco*RI and ligated into pcDNA3, creating pcDNA3-hOCT1-V5His. All DNA sequencing was performed by the Arizona Research Laboratory–Laboratory of Molecular Systematics and Evolution (University of Arizona, Tucson, AZ).

The pcDNA3-hOCT1-V5His was linearized with *Pvu*I and transfected into HeLa cells using Effectine (QIAGEN, Valencia, CA) according to the manufacturer's instructions (with the exception that we used a cDNA-to-enhancer ratio of 1:8, mass/volume). Transfected cells were plated at ~50% confluence and the medium was changed 18 to 24 h later. At 72 h after transfection, the HeLa cells were exposed to, and thereafter continuously grown in, culture media containing 400 μg/ml G418 (Inivtrogen) to select for cells that had incorporated the cDNA construct. To select cells stably expressing OCT1 transport activity, the cells were exposed to 20 μM NBD-TMA, a fluorescent organic cation (or a pH-insensitive derivative of NBD-TMA (Bednarczyk et al., 2000)), for 20 min, then trypsinized and resuspended in phosphate-buffered saline plus 250 μM TPrA. The subpopulation of fluorescent cells was sorted using a fluorescence-activated cell sorter (Arizona Research Laboratories, Tucson AZ). From the reclaimed cells, individual clones were selected by dilution cloning. HeLa cells were also stably transfected with the wild-type hOCT1 in pcDNA3.1 (i.e., without addition of the C-terminal V5His sequence) using the same general method.

HeLa cells stably transfected with pcDNA3-hOCT1-V5His or pcDNA3.1-hOCT1 were cultured at 37° in a humidified 95% air/5% CO_2 environment. The growth media used to maintain the cells was RPMI 1640 supplemented with 2 mM glutamine, 50 U/ml penicillin, 50 μg/ml streptomycin, and 400 μg/ml G418. Cells were trypsinized (trypsin + 0.25 mM EDTA; Invitrogen) and seeded at ~600,000 or ~300,000 cells/well of a 12-well culture plate (Falcon or Cell Star) and transport experiments were performed 2 or 3 days later, respectively.

Fluorescence of NBD-TMA$^+$ Loaded Cells. HeLa cells stably transfected with pcDNA3-hOCT1-V5His were loaded with 10 to 20 μM NBD-TMA in Waymouth buffer (135 mM NaCl, 13 mM HEPES, 2.5 mM $CaCl_2$, 1.2 mM $MgCl_2$, 0.8 mM $MgSO_4$, 5 mM KCl, and 28 mM glucose) for 5 to 30 min. The solution was then aspirated and the cells were rinsed with Waymouth buffer plus 100 to 250 μM TPrA and maintained in this solution during fluorescence microscopy.

Measurement of Transport. After aspiration of the culture medium, the cells in each well of a 12-well plate were twice exposed, each time for 15 min, to 1 ml of Waymouth buffer at room temperature. After the second 15-min incubation, the buffer was aspirated and Waymouth buffer containing 1 μCi/ml [^{3}H]TEA, with or without inhibitor, was added. After a prescribed interval, the buffer containing radiolabeled substrate was aspirated and the cells were washed twice with 1 ml of ice-cold Waymouth buffer. The cells were then solubilized with 1 ml of 0.2 N NaOH and 1% SDS. This solution was pipetted repeatedly until homogenous, then neutralized with 200 μl of 1 N HCl. Ten milliliters of scintillation cocktail were then added to this homogenate, and radioactivity in the resulting solution was counted in a scintillation counter. The cells in each of three additional wells were counted using a cell counter (Beckman Coulter, Fullerton, CA) and the counts averaged to determine the number of cells per well (routinely 1.0–1.2 million cells/well). Cells in three additional wells were solubilized with 1 ml of 0.2 N NaOH later neutralized with 200 μl of 1 N HCl and used to determine the average protein content of each well (Bio-Rad, Hercules, CA). The concentration of inhibitor that reduced uptake by 50% (IC_{50}) was generated using Sigma Plot by fitting the data to the following equation (Groves et al., 1994): $J = [(J_{app}\,[T])/(IC_{50} + [I])] + C$, where J is the uptake of [^{3}H]TEA; J_{app} is a constant related to the product

of the maximal rate of TEA uptake and the ratio of the inhibitor IC_{50} and the K_t for TEA transport; [T] is the concentration of [^{3}H]TEA; [I] is the inhibitor concentration, and C is a constant representing the nonsaturable component of [^{3}H]TEA uptake.

Modeling with Catalyst and Cerius^2. The computational molecular modeling studies were carried out using Silicon Graphics Octane workstations (SGI, Mountain View, CA). The 3D structures of substrates were built interactively using either Catalyst version 3.1 or 3.4. (Accelrys, San Diego, CA) and used to generate a 3D-QSAR model. The number of conformers generated for each substrate was limited to a maximum of 255 with an energy range of 20 kcal/mol. Ten hypotheses were generated using conformers for the 22 molecules in the training set and the IC_{50} values, after manual selection of the hydrogen bond donor, hydrogen bond acceptor, hydrophobic, and negative ionizable pharmacophoric features. After assessing all 10 hypotheses generated, the lowest energy cost hypothesis was considered the best. The goodness of the structure-activity correlation was estimated from calculated r values. Statistical significance of the retrieved hypothesis was verified by permuting the response variable; i.e., the activities of the training set compounds were mixed a number of times (so that each value was no longer assigned to the original molecule) and the Catalyst hypothesis generation procedure was repeated. Multiple conformations of the eight molecules in the test set were generated using the same method as the training set before fitting the conformers to the pharmacophore to generate a prediction.

Cerius^2 (Accelrys) was used to generate more than 200 molecular descriptors for the 30 molecules used in the Catalyst studies. The forward stepwise regression method incorporated within Cerius^2 was then used to relate the log IC_{50} to a selection of these descriptors, and hence result in a QSAR model. The model was validated for numerical stability and internal consistency using both the leave-one-out cross-validation method and by permuting, or randomizing, the response variable.

Results

hOCT1 Sequence Variation and Stable Cell Line Characteristics. The sequence of the hOCT1 cDNA provided by K. Giacomini differed by one base from the sequence reported by Zhang et al. (1997) (Genbank accession number U77086). That difference was a guanine, rather than an adenine, at nucleotide 1275. The resulting codon encoded a valine rather than a methionine at amino acid 408. The sequence of an hOCT1 fragment (from position 1197 to 1588), amplified using RT-PCR from human renal mRNA, confirmed the presence of G at position 1275 (i.e., valine at amino acid 408) in a sequence that otherwise matched that of Zhang et al. (1997). The full-length cDNA coding for hOCT1, as provided by Dr. Giacomini, was therefore used for the preparation of the hOCT1-V5His construct employed in the studies described below.

Figure 1A shows cells stably transfected with pcDNA3-hOCT1-V5His after a 10-min exposure to 20 μM NBD-TMA. Figure 1B is a fluorescence image of the same cells, showing that only a fraction of the transfected cells that were resistant to G418 actually transported NBD-TMA. Cells transfected with hOCT2, rbOCT1, and rbOCT2 also showed increased fluorescence after exposure to NBD-TMA (data not shown). In fact, only 5 to 10% of the 'parent' population of cells expressed transport activity. Cells positive for hOCT1-V5His-mediated transport of NBD-TMA were selected using 1) flow cytometry, 2) dilution-cloning, and 3) cloning rings and discs. Figure 1C shows [^{3}H]TEA uptake data from wild-type HeLa cells, the parent cell population, and cells selected from the parent cell line. The parent cell population showed about twice as much radiolabeled TEA accumulation as the wild-type HeLa cells. After selection of NBD-TMA–containing cells using flow cytometry, there was a 6-fold increase in accumulation of radiolabeled TEA. The remaining studies reported here used a clonal cell line selected from this population.

Figure 2A shows the time course of [^{3}H]TEA uptake into HeLa cells stably expressing hOCT1-V5His. TEA uptake was approximately linear for 5 to 7 min, and a 5-min uptake provided a reasonable estimate of the initial rate of transport. Figure 2B shows the effect of increasing concentrations of unlabeled substrate on the rate of hOCT1-mediated transport of TEA from which the kinetics of transport of this substrate was estimated. In three separate experiments, the apparent K_t for TEA transport was 164 $\pm$ 17.9 μM, with a J_{max} of 3.5 $\pm$ 0.33 nmol mg^{-1} 5 min^{-1}. These values are comparable with those reported by Zhang et al. (1998) in their study of hOCT1-mediated transport in transiently transfected HeLa cells. Consequently, we elected to use the transport of TEA, and the inhibition of TEA transport, in the remaining studies. We also measured the kinetics of TEA transport in cells stably expressing the wild-type hOCT1 (i.e., without the V5His tagged sequence; data not shown). In these experiments, the K_t for TEA transport in the wild-type clones was similar to that of the tagged protein, suggesting that the presence of the V5His sequence at the C terminus of hOCT1 had no significant effect on the interaction of substrate with the transport binding site. Hereafter, hOCT1-V5His is referred to simply as hOCT1.

To further assess the kinetic characteristics of our hOCT1 cell line, we examined the inhibition of hOCT1-mediated TEA transport produced by a series of tetraalkylammonium compounds (nTAAs: TEA, TPrA, TBA, and TPeA). The IC_{50} for each compound was determined by measuring the 5-min accumulation of [^{3}H]TEA in the absence or presence of five incremental concentrations of inhibitor (Table 1). Figure 2C plots the relationship between the log of the measured IC_{50} values for the test agents and their calculated Log P values (CLog P), confirming the existence of a strong correlation between hydrophobicity and IC_{50} for the nTAAs commonly used in organic cation studies. Additionally, the IC_{50} values for these compounds compared favorably with those reported previously for nTAA inhibition of hOCT1 expressed in HeLa cells (Zhang et al., 1999) and *Xenopus laevis* oocytes (Dresser et al., 2000).

Pharmacophore 3D-QSAR Generation. We next used a computational approach to develop QSARs and a predictive model of inhibitor/hOCT1 interaction. The commercial software program Catalyst was used to model the structural features that facilitate interaction of inhibitors at the hOCT1 binding site. A set of chemically diverse molecules with IC_{50} values for hOCT1 spanning more than 3 orders of magnitude (Table 2) was used for pharmacophore construction. These 22 molecules identified a pharmacophore with four features of interaction with the transporter. The four features included a positive ionizable feature and three hydrophobes at distances of 5.12, 4.19, and 5.32 Å from the center of the positive ionizable feature (Fig. 3A). Regression of the logs of experimentally determined and the estimated IC_{50} values for the compounds contributing to the model resulted in a correlation coefficient of 0.86 (Fig. 4, ●; Table 2). Compounds with

TABLE 1
IC_{50} values for selected nTAA compounds against [^{3}H]TEA transport in hOCT1-expressing HeLa cells (mean ± S.E.M.; n = 3 to 4).

Compound	CLog P	IC_{50}
		μM
TEA	−3.14	167.5 ± 25.9
TPrA	−1.02	22.0 ± 4.1
TBA	1.09	6.5 ± 1.5
TPeA	3.21	1.8 ± 0.2

the highest apparent affinity for the transporter (i.e., those with the lowest IC_{50} values) generally possessed the greatest number of pharmacophore features, whereas compounds with structures that included fewer of these features generally showed a lower apparent affinity for the transporter. This can be seen in Fig. 3B, where the most potent inhibitor, clonidine, (IC_{50} = 0.71 μM) is characterized by all four pharmacophore features, but the least potent inhibitor, choline (IC_{50} = 3.5 mM), is described by only one of the features, (i.e., the positive ionizable feature) (Fig. 3C). Additionally, choline has a hydrogen bond donor near two of the hydrophobes, perhaps contributing to its failure to inhibit TEA transport to a significant degree. Although many of the chemical features of the diverse group of molecules in the training set were in spatial agreement with the model pharmacophore, some molecular structures clearly lay outside the area described by the model. This can be readily seen for ranitidine (IC_{50} = 21.7 μM; Fig. 3D). Furthermore, there was generally poor correlation (r = 0.54) between the Catalyst-produced estimates of IC_{50} and the experimentally determined values for the pyridinium- and quinolinium-based set of substrates described in the following group of experiments (Fig. 4, ○; Table 2). Nevertheless, the Catalyst-produced model was more accurate than the often-cited correlation between the hydrophobicity of substrates or inhibitors and the apparent affinity of OC transporters for these compounds. Figure 5 shows the relationship between the log of the IC_{50} for each of the members of the training set and their CLog P values. The correlation (r = 0.73) was less than that of the Catalyst model (r = 0.86), which may reflect the substantial variation in the three dimensional structure of several inhibitors with similar CLog P values. Indeed, when a structurally homologous group of molecules is examined (e.g., the nTAAs), the corre-

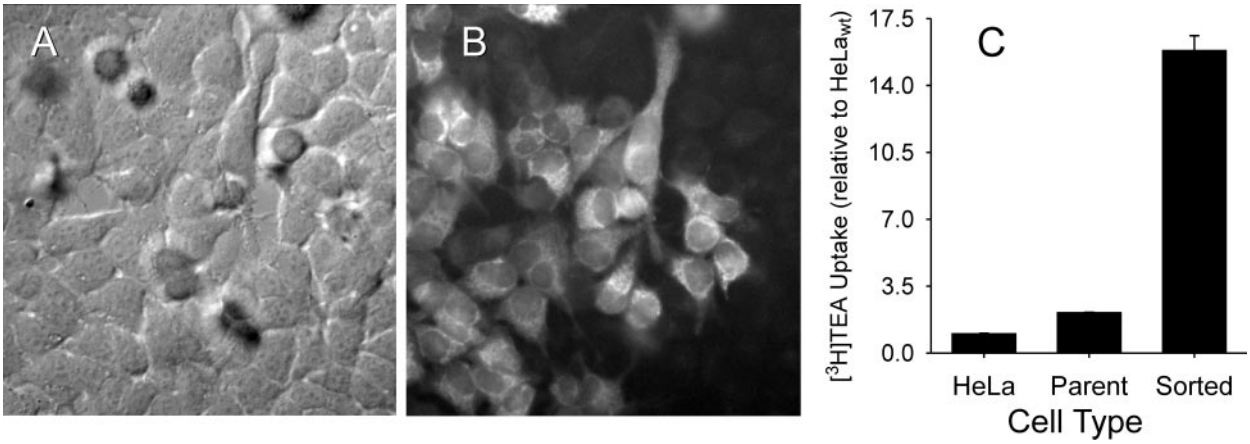

Fig. 1. A, differential interference contrast image (400×) of HeLa cells stably transfected with pcDNA3.1-hOCT1 after a 10 min exposure to 20 μM NBD-TMA$^+$ (note the elongated cell for reference). B, fluorescence image of the same field of view showing NBD-TMA$^+$ accumulation in a subpopulation of these cells. C, Accumulation of 0.04 μM [^{3}H]TEA$^+$ by untransfected wild-type HeLa cells ($HeLa_{wt}$), HeLa cells stably transfected with pcDNA3-hOCT1-V5His (Parent), and cells sorted from the parent cell population by flow cytometry (Sorted). The height of each bar indicates the mean (± S.E.) of 60-min uptakes measured in three confluent wells (~1 × 10^6 cells).

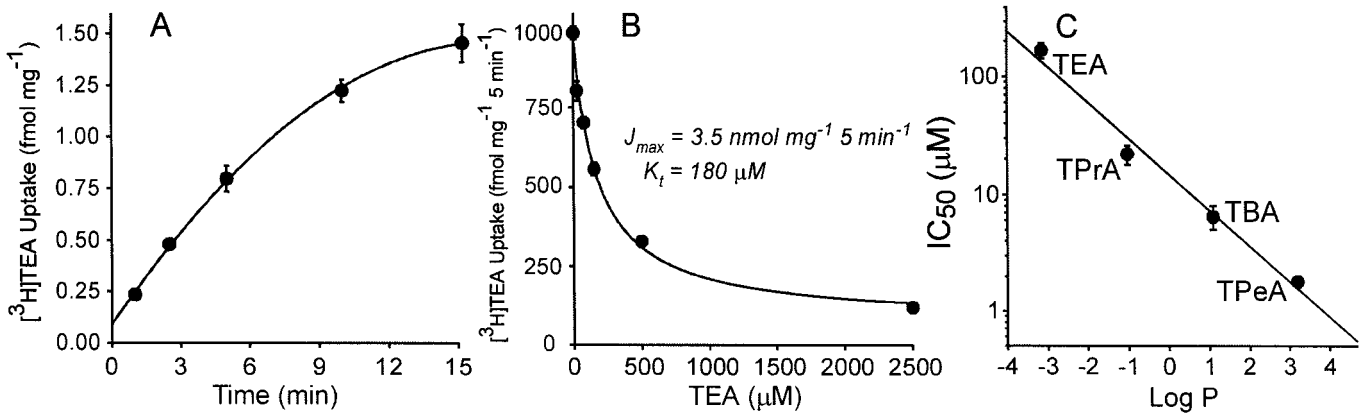

Fig. 2. Kinetic data acquired from HeLa cells stably transfected with pcDNA3-hOCT1-V5His. In each plot, the solid points represent the mean (± S.E.) of uptakes measured in three confluent wells of cells in a single, representative experiment. A, time-dependent accumulation of 0.04 μM [^{3}H]TEA$^+$. B, kinetics of hOCT1-mediated TEA transport as shown by the profile in inhibition of 0.05 μM [^{3}H]TEA$^+$ uptake produced by increasing concentrations of unlabeled TEA$^+$ (Malo and Berteloot, 1991). The curve was fit to the data using a nonlinear regression algorithm (SigmaPlot, v3.0). C, relationship between calculated hydrophobicity (Log P) of nTAAs and the measured IC_{50} each displayed against hOCT1-mediated TEA uptake. Each point represents the mean (± S.E.) of IC_{50} values calculated in three separate experiments.

TABLE 2
Observed and predicted IC_{50} values from computational models for a structurally diverse array of organic cations
Kinetic parameters were measured against [^{3}H]TEA transport in hOCT1-expressing HeLa cells (mean ± S.E.M.; n = 3 to 5).

Compound	IC_{50}	Catalyst Prediction	Cerius^2 Prediction	CLog P
	μM	μM	μM	
Training Set				
Clonidine	0.71 ± 0.08	3.1	1.8	3.08
TPeA	1.8 ± 0.2	1	2.2	3.21
Chlorpromazine	4.3 ± 0.16	6.4	2.8	6.15
Quinidine	5.4 ± 0.22	4.5	7.1	3.24
TBA	6.5 ± 1.5	1.8	9.7	1.09
Crystal violet	7.7 ± 1.94	9	3.1	6.25
Pindolol	9.7 ± 0.94	7.6	4.5	—[a]
Procainamide	14.5 ± 0.83	8.4	18.9	1.00
1-Methyl-4-phenylpyridinium	15.7 ± 1.15	93	25.6	−2.31
Amantadine	18.4 ± 2.42	73	25.0	2.04
Ranitidine	21.7 ± 2.33	2.4	11.2	1.31
TPrA	22 ± 4.1	7.4	45.1	−1.02
Nicotine	53.2 ± 9.07	71	81.7	1.97
1-(2-Hydroxyethyl)quinolinium	80.6 ± 3.2	73	67.6	−2.32
Tyramine	107 ± 6.7	71	187	0.81
TEA	168 ± 25.9	720	116	−3.14
Thiamine	434 ± 31.5	75	702	−5.04
Dopamine	487.2 ± 43.3	71	359	0.21
Cyclohexylamine	544 ± 19.0	76	187	1.41
N^1-Methylnicotinamide	1035 ± 58.0	720	457	−5.21
Histamine	3007 ± 27.2	720	1771	—[a]
Choline	3540 ± 24.0	720	5409	−4.36
Test Set				
1-(2-Hydroxyethyl)-4-phenylpyridinium	16.2 ± 1.4	85	38.3	−1.81
1-Ethyl-4-phenylpyridinium	7.1 ± 1.1	92	13.9	−1.78
1-(Phenyl)methyl-4-phenylpyridinium	9.3 ± 0.6	28	8.4	−0.54
1-(2-Hydroxyethyl)-3-phenylpyridinium	31.1 ± 2.3	71	63.5	−1.81
1-Ethyl-3-phenylpyridinium	28.3 ± 4.5	71	9.4	−1.78
1-(Phenyl)methyl-3-phenylpyridinium	5.5 ± 0.9	14	11.4	−0.54
1-Ethylquinolinium	67.6 ± 11.2	75	21.3	−2.29
1-(Phenyl)methylquinolinium	14.3 ± 0.7	22	11.5	−1.05

[a] The CLogP program was unable to calculate Log P for pindolol and histamine.

lation between hydrophobicity and apparent affinity for hOCT1 can be quite striking (Fig. 5, ○).

Descriptor-Based QSAR Generation. Previous work has shown that a descriptor-based QSAR model generated using Cerius^2 can be superior in its ability to predict activity parameters than a Catalyst-derived model (Ekins and Obach, 2000). Consequently, a descriptor-based QSAR model for hOCT1 was built using the molecular descriptors generated by the Cerius^2 program. The following equation identifying molecular descriptors found to be correlated with inhibition of hOCT1 activity was produced using forward stepwise regression:

$$\text{Log } IC_{50} = 3.94081 - 0.212694 \times \text{S\_ssNH} + 0.458416 \times \text{ADME\_solubility} - 0.0725515 \times \text{Jurs-RNCS} - 0.363722 \times \text{Shadow-}\nu - 0.0899946 \times \text{Atype\_H\_52}$$

in which S_ssNH defines an E-state key for sum of nitrogens connected to a hydrogen and to two single bonds (Ghose et al., 1998); ADME solubility is a descriptor for prediction of aqueous solubility; Jurs-RNCS is related to the negative charge surface area mapped over the solvent-accessible surface area of individual atoms; Shadow-ν is a member of the shadow indices descriptors and is the ratio of largest to smallest dimension; and Atype_H_52 is the number of times that each AlogP atom appears in the molecule and is part of the Thermodynamic family (AlogP_atypes) of descriptors (Viswanadhan et al., 1989). The correlation of the experimentally determined (Log) IC_{50} values and those predicted for the descriptor-based model described in eq. 1 generated a correlation coefficient of 0.95 (Fig. 6). After permuting the log data with the descriptors and attempting to generate eqs. 9 times (to give 90% confidence in the models produced), the mean r value was 0.65 ± 0.14, which represented 2.1 S.D. from the r value described for the model in eq. 1

Interaction of *N*-1-Substitued Pyridiniums and Quinoliniums with hOCT1. Of the five molecular descriptors presented in eq. 1, the relative importance of the Shadow-ν term (i.e., the ratio of the largest to the smallest dimension of the inhibitor) was particularly intriguing. In a previous study, we used a series of phenylpyridinium and quinolinium compounds to examine the influence of the spatial distribution of hydrophobic mass on the interaction of inhibitors with the OC/H^+ exchanger of rabbit renal brush border membrane vesicles (Wright and Wunz, 1999). Of relevance to the present observations is the fact that the ratio of the largest to the smallest dimension (Shadow-ν values) of these compounds varies systematically. The QSAR model presented in eq. 1 suggests that systematic variation of molecular dimension should have a predictable influence on the interaction of test agents with hOCT1. Consequently, we elected to investigate the inhibitory efficacy of a group of phenylpyridinium and quinolinium compounds with ethyl, hydroxyethyl, or methylphenyl side groups located at the N1 position (Fig. 7).

The present work, and results from previous studies (e.g., Ullrich et al., 1992; Wright et al., 1995) led to the hypothesis that the IC_{50} values of the test agents would vary inversely

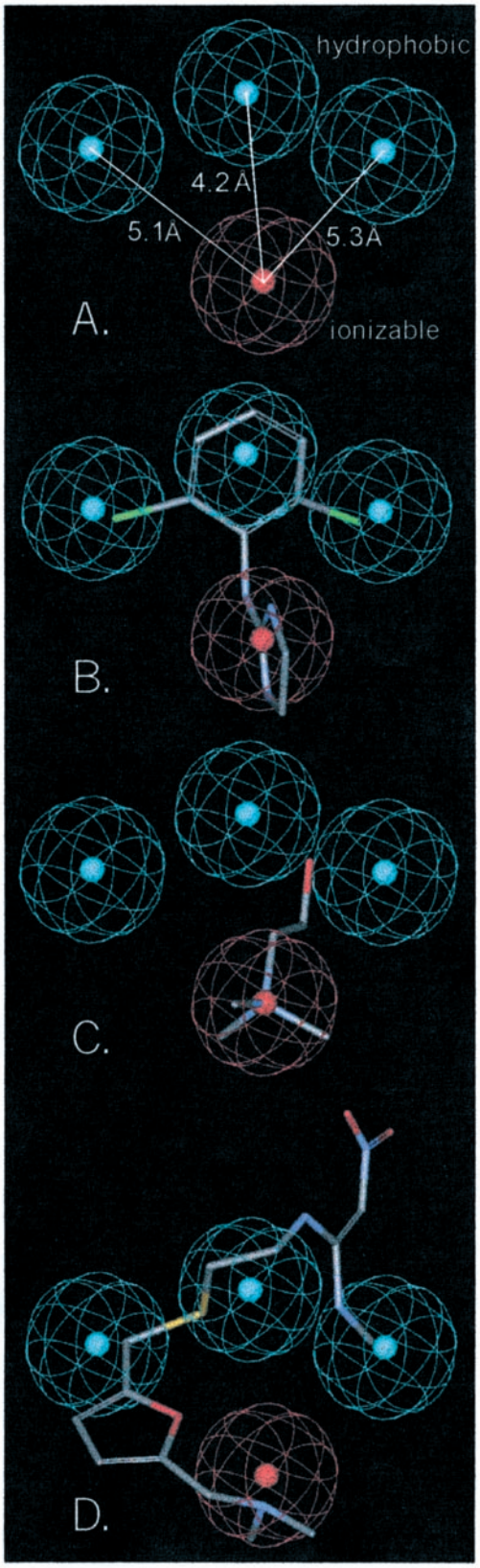

Fig. 3. A, the structure of the Catalyst-produced pharmacophore illustrating three hydrophobic areas (cyan) and a positive ionizable feature (red). B, clonidine mapped to the pharmacophore model. C, choline mapped to the pharmacophore model. D, ranitidine mapped to the pharmacophore model.

with hydrophobicity. This was generally the case for each 'genus' of chemical (i.e., 4-phenylpyridiniums, 3-phenylpyridiniums, and quinoliniums): for each 'species' within a given genus, increasingly hydrophobic residues at the N1 position were associated with a decrease in IC_{50} for hOCT1-mediated TEA transport (Fig. 8). However, there was systematic variation in the apparent affinity of hOCT1 for the different structural groups. The more elongated 4-phenylpyridiniums consistently had lower IC_{50} values for hOCT1 than did the

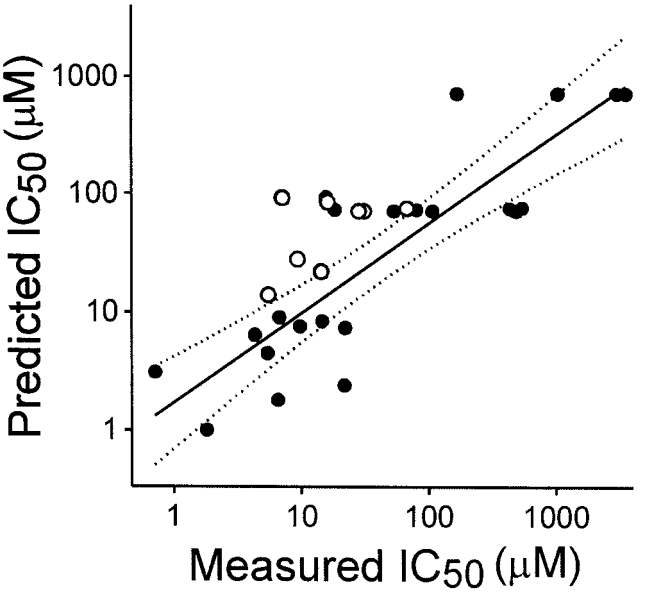

Fig. 4. The relationship between the Catalyst-predicted IC_{50} values and the measured IC_{50} values. The solid line describes the linear regression of the data representing the 22 molecules comprising the training set (●; r = 0.86); the dotted lines illustrate the 95% confidence interval of the regression. ○, the eight molecules from the test set (r = 0.54).

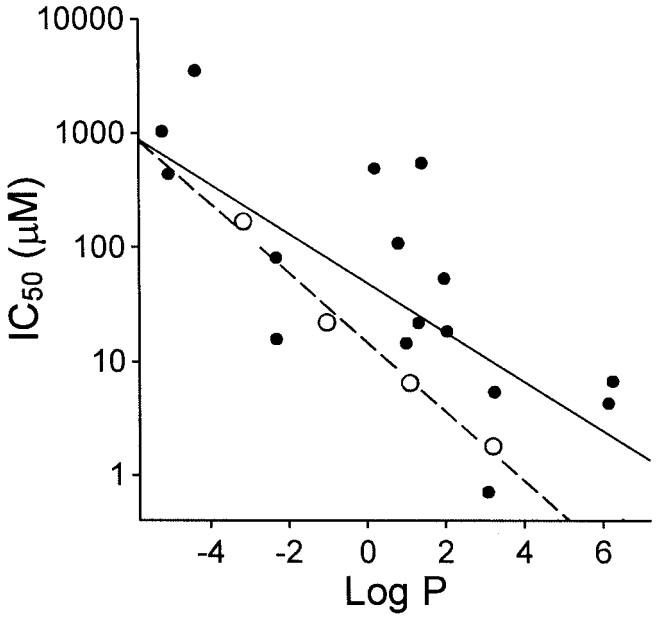

Fig. 5. Relationship between observed IC_{50} and calculated hydrophobicity (Log P) for the training set of compounds used to generate the Catalyst-produced pharmacophore. The solid line depicts the linear regression of these data (r = 0.73), and the dotted lines show the 95% confidence interval for the regression. The dashed line depicts the linear regression for a subset of these data (i.e., the nTAAs) (r = 0.99). Each point is the mean of measurements made in three or four separate experiments.

3-phenylpyridiniums, which, in turn, had lower IC_{50} values than the least linear compounds, the quinoliniums (Fig. 8; Table 2). This observation suggests that, although hydrophobicity is clearly an important determinant of molecular interaction with hOCT1, changes in molecular dimension can also predictably influence apparent affinity of the transporter for a molecule.

In a previous study of the influence of planar hydrophobic mass on the binding of OCs to the luminal OC/H exchanger of rabbit renal BBMs (Wright and Wunz, 1999) we noted that, in general, planar substrates bind with greater affinity to the exchanger than nTAA compounds of comparable hydrophobicity. Indeed, there is a marked discrepancy between hydrophobicity and binding efficacy between nTAAs and the selected pyridinium/quinolinium compounds at the luminal OC/H^+ exchanger. This led to the hypothesis that the globular (rather than planar) nature of nTAAs places a substantial fraction of their hydrophobic mass away from the postulated planar binding surface of the OC/H^+ exchanger, in contrast to the situation afforded by planar substrates. No such discrepancy was noted between the interactions of these two groups of compounds with hOCT1 (inset, Fig. 8). To extend the examination of the influence of globular, rather than planar, hydrophobic mass on interaction with hOCT1, the inhibitory efficacies of two compounds used in the development of the computational model were compared. Cyclohexylamine and amantadine are unsaturated hydrocarbons with a primary amine-containing side group. Importantly, the structure of cyclohexylamine is fully contained within amantadine, with the latter containing additional hydrophobic mass that is supraplanar to a postulated binding surface (refer to Fig. 7). Amantadine is known to be a substrate of basolateral OC transport in intact rat tubules (Wong et al., 1990), and it is likely that cyclohexylamine, which is a substructure of amantadine, is also a substrate. Interestingly, the presence of additional, nonplanar hydrophobic mass increased the inhibitory effectiveness of amantadine 25-fold over that observed for cyclohexylamine (IC_{50} values of 19 and 540 μM, respectively; see Table 2).

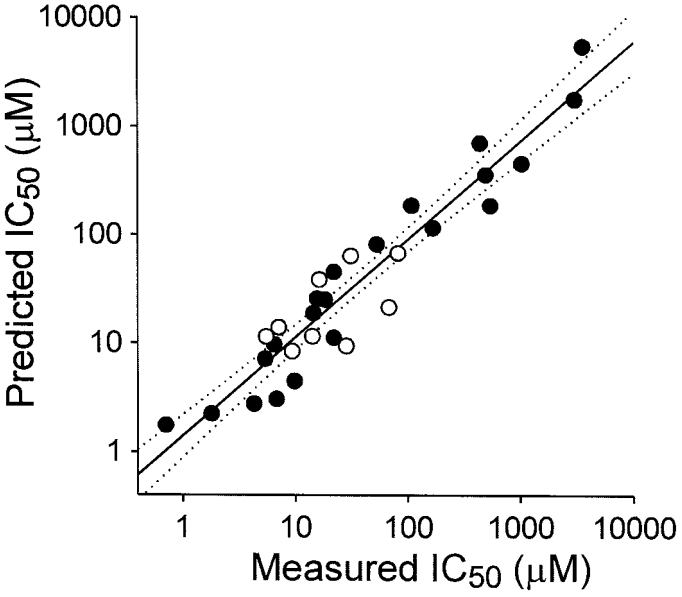

Fig. 6. The relationship between the Cerius 2 predicted IC_{50} values and the measured IC_{50} values. The solid line describes the linear regression of the data representing all 30 molecules used in the present study (r = 0.95); the dotted lines illustrate the 95% confidence interval of the regression. ○, the eight molecules from the test set.

Discussion

Although the interaction of substrate with OC transporters has been described for a variety of different compounds (e.g., Dresser et al., 2001), such descriptions have usually lacked structural/spatial information with regard to the substrates or transporters. Structure-related analysis of substrate interaction with cloned OC transporters has been performed using the nTAAs (Zhang et al., 1999; Dresser et al., 2000). These compounds, however, have limited structural diversity. In the present study, two groups of chemicals were employed, one with broad structural diversity and binding affinity for hOCT1, and a second of comparatively limited structural breadth that focused on the influence of a single structural parameter. Both groups were used to extend the

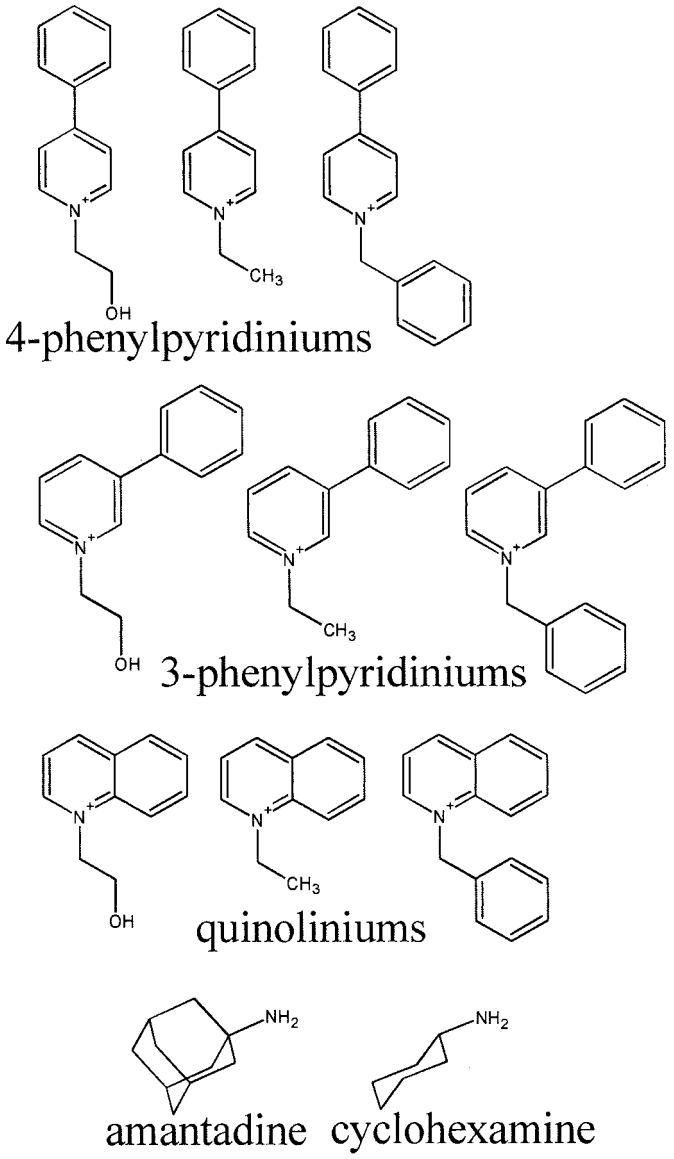

Fig. 7. Structural formulae of the molecules used to assess the influence of the Shadow-ν dimensional descriptor on hOCT1-mediated TEA transport.

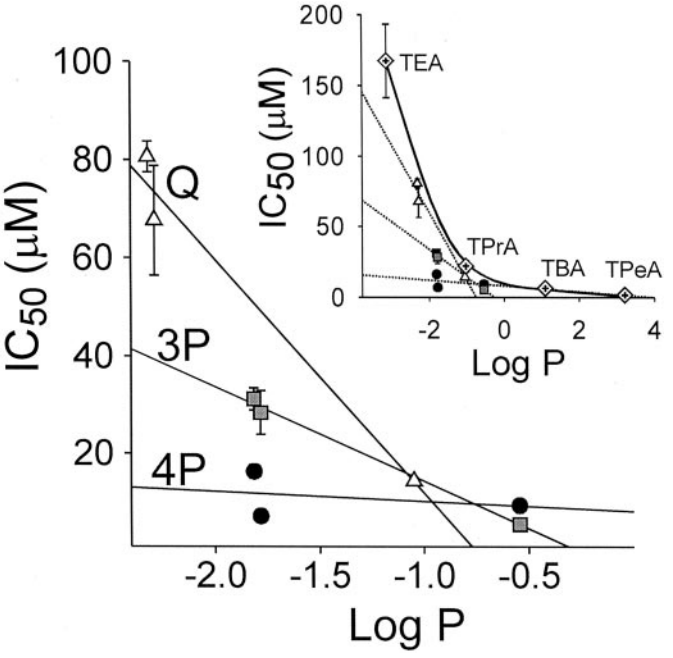

Fig. 8. The relationship between the IC_{50} for inhibition of hOCT1-mediated [^{3}H]TEA transport and the calculated hydrophobicity (Log P) of the members of the three sets of test compounds: 4-phenylpyridiniums (4P, ●); 3-phenylpyridiniums (3P, ▨); and quinoliniums (Q, △). Each point is the mean (± S.E.) of IC_{50} values measured in three or four separate experiments. Inset, within each set of test agents, Log P was systematically increased by altering the N^1-substituent (-2-hydroxyethyl to -ethyl to -(phenyl)methyl; see Fig. 7). The relationship between the IC_{50} for inhibition of hOCT1-mediated [^{3}H]TEA transport and the calculated hydrophobicity (Log P) of the three sets of test compounds, and the nTAA compounds (◇).

observation that substrate hydrophobicity is a principal determinant of substrate interaction with OC transporters by identifying distinct structural features that influence molecular interaction with the human ortholog of the organic cation transporter, OCT1.

To achieve this, a computational method was used to generate a pharmacophore reflecting the structural features that maximize substrate-transporter interaction. Such methods use conformers of ligands to suggest functional groups, the geometry of structural features, regions of favorable/unfavorable electrostatic interaction, or favorable/unfavorable steric interactions that may be essential for activity or fit to the receptor binding/active site. The combination and 3D spatial distribution of physicochemical properties, the functional groups of the ligands, and a measure of binding site properties of an enzyme, such as the K_m (apparent) (Nelsestuen and Martinez, 1997), K_i, IC_{50}, or other measure, are used to define the 'pharmacophore'. We used the commercial software package, Catalyst, to develop a pharmacophore for hOCT1 that was based upon the inhibition of transport activity produced by a structurally diverse array of molecules. The IC_{50} values produced by this training set spanned more than 3 orders of magnitude (Table 2). The pharmacophore developed from this set of compounds was composed of one positive ionizable feature and three distinct hydrophobes, characteristics that are qualitatively consistent with previously reported observations demonstrating the importance of a basic nitrogen and a diffuse hydrophobic component(s) for interaction with organic cation transporters (Ullrich, 1999; van Montfoort et al., 2001;Ullrich, 1997). The Catalyst-derived pharmacophore also provided valuable information regarding the geometry of these features relative to one another, and the resulting model had a strong internal correlation between measured and predicted IC_{50} values (r = 0.86). The strong internal correlation between the measured and the predicted IC_{50} values reported here for the training set compares favorably with recently developed Catalyst-derived pharmacophores for another xenobiotic transporter, P-glycoprotein (Ekins et al., 2002).

Examination of the values in Fig. 4, however, did reveal some significant discrepancies between measured and predicted IC_{50} values, especially for members of the several phenylpyridinium compounds in the test set. Although these discrepancies may have reflected, at least in part, the limited structural diversity of the molecules in the test set, significant discrepancies were also noted within the training set (e.g., for amantadine and ranitidine; Table 2). In retrospect, the presence of 'outliers' in a pharmacophore-based model is not surprising. The algorithm used to develop a pharmacophore seeks a single, best-fit structure for interaction with a receptor that is expected to possess a marked degree of structural specificity. However, OC transporters do not display the narrow specificity of the typical receptor, which generally accepts a 'best' structure to the exclusion of most others. OC transporters in contrast, because of the protective role they play, necessarily must accept a broad array of substrate structures, including compounds to which the host organism may never have been exposed (e.g., a dietary toxin or synthetic drug). Therefore, one might predict a selective advantage arising from a process that can interact effectively with a diverse array of environmental chemicals, making it desirable for OC transporters to accept chemical structures that fit a generalized format, rather than one represented by a classic pharmacophore.

To achieve a computational model with greater predictability, a descriptor-based QSAR model was subsequently derived using Cerius^2. In contrast to the structurally based pharmacophore approach, the QSAR regression model was based upon multiple regression of a number of quantitative molecular descriptors. The final model emphasized the importance of hydrophobic (ADME_solubility), hydrogen bond donor (S_ssNH), shape (Shadow-ν), and charge (Jurs-RNCS) features. The Cerius^2 model had a very high correlation between measured and predicted IC_{50} values for all 30 molecules evaluated in this present study (Fig. 6; r = 0.95) and represented a marked improvement in predictability compared with the Catalyst, pharmacophore-based model, as well as with previous efforts to correlate OCT binding to the single physical descriptor, CLogP.

Not surprisingly, greatest weight in the QSAR model was given to a molecular descriptor associated with hydrophobicity (ADME solubility). Somewhat unexpected, however, was the next most heavily weighted term, Shadow-ν (ratio of the longest to shortest molecular dimension). This dimensionality term, Shadow-ν, describes a physical parameter not previously hypothesized to significantly contribute to molecular interaction with OC transporters. This term clearly distinguishes the phenylpyridinium and quinolinium compounds included in this study, and presumably explains the improved correlation of predicted and measured IC_{50} values for the test set compounds evident in the Cerius^2 QSAR model

(Fig. 6), compared with the Catalyst pharmacophore model (Fig. 4).

Differences in relative geometric location of planar hydrophobic mass are intrinsic in the structures of the phenylpyridinium and quinolinium compounds used in this study. These changes in the geometric location of planar hydrophobic mass permitted a systematic assessment of the potential role that steric configuration can play in binding of substrate to an OC transporter. In fact, although for any chemical genus tested (i.e., 4-phenyl or 3-phenylpyridinium or quinolinium) increases in hydrophobicity (introduced through the *R*-group at the N1 position) were associated with decreases in IC_{50} (Fig. 8), it was also evident that the location of planar hydrophobic mass had a clear and systematic effect on inhibitor interaction. For molecules of similar hydrophobicity, the rank order of apparent affinity for hOCT1 was 4-phenylpyridinium > 3-phenylpyridinium > quinolinium, which corresponded to the rank order of the mean Shadow-ν values for each genus: 2.45 > 2.05 > 1.75, respectively. Although the basis for this effect is not clear, it may reflect a systematic misalignment of chemical features, such as the positive charge, with important structural elements of the binding site, resulting in decreased affinity for the molecule. Alternatively, the more elongated structure of the 4-phenylpyridiniums may permit association with a more stabilizing region of the binding site than the foreshortened quinoliniums. Additionally, it is possible that the hypothesized stabilizing feature of the protein is fundamental for π-π stacking type interactions with the phenyl group of the more elongated 4-phenylpyridiniums, and perhaps this stabilizing feature is misaligned or not adequately reached by the unsaturated rings within the other two groups of compounds.

Interestingly, the phenylpyridinium and quinolinium compounds used in the present study produced a very different inhibitor profile in a previous study on the molecular determinants of substrate interaction with the OC/H^+ exchanger of renal brush border membranes (Wright and Wunz, 1999). Whereas for hOCT1, a change in molecular dimension (basis for the shift in the Shadow-ν term) produced the marked effect on binding site interaction evident in Fig. 8, these structural changes had no effect on interaction with the OC/H^+ exchanger, leading to the suggestion that the OC/H^+ exchanger has a receptor surface that is, in functional terms, broadly planar in structure (Wright and Wunz, 1999). The present results suggest that the hOCT1 receptor is not necessarily represented by a broad plane. In fact, the substantially higher affinity of hOCT1 for amantadine, compared with cyclohexylamine (Table 2), suggests that the binding site for hOCT1 may be best described as a 'pocket' that is conducive to establishing hydrophobic interactions above the previously hypothesized hydrophobic plane.

In summary, a Catalyst-derived pharmacophore confirmed the importance of positive charge and hydrophobicity on binding of substrates to OC transporters and extended upon those observations by providing geometric location of the features relative to one another. A QSAR model derived using Cerius^2 reiterated the importance of hydrophobicity and a basic nitrogen to molecular interaction with organic cation transporters. More importantly, the QSAR analysis unveiled a structural parameter (dimensionality) not previously hypothesized to have value in the molecular interaction with an organic cation transporter. The importance of this dimensionality parameter was validated by the empirical test of the effect of the placement of planar hydrophobic mass on binding to hOCT1. The developing view is of an hOCT1 binding site that is most conducive to interaction with comparatively elongated, cationic molecules capable of interacting with a supraplanar stabilizing structure within a hydrophobic pocket of the protein.

Acknowledgments

We gratefully acknowledge the assistance Dr. Eugene Mash (University of Arizona Dept. of Chemistry) for his assistance in the synthesis of NBD-TMA and the several phenylpyridinium and quinolinium compounds used in this study.

References

Bednarczyk D, Mash EA, Aavula BR, and Wright SH (2000) NBD-TMA: a novel fluorescent substrate of the peritubular organic cation transporter of renal proximal tubules. *Pflueg Arch Eur J Physiol* **440:**184–192.

Dresser MJ, Gray AT, and Giacomini KM (2000) Kinetic and selectivity differences between rodent, rabbit and human organic cation transporters (OCT1). *J Pharmacol Exp Ther* **292:**1146–1152.

Dresser MJ, Leabman MK, and Giacomini KM (2001) Transporters involved in the elimination of drugs in the kidney: organic anion transporters and organic cation transporters. *J Pharm Sci* **90:**397–421.

Ekins S, Kim RB, Leake BF, Dantzig AH, Schuetz EG, Lan LB, Yasuda K, Shepard RL, Winter MA, Schuetz JD, et al. (2002) Three-dimensional quantitative structure-activity relationships of inhibitors of p-glycoprotein. *Mol Pharmacol* **61:**964–973.

Ekins S and Obach RS (2000) Three-dimensional quantitative structure activity relationship computational approaches for prediction of human in vitro intrinsic clearance. *J Pharmacol Exp Ther* **295:**463–473.

Ghose AK, Viswanadhan VN, and Wendolowski JJ (1998) Prediction of hydrophobic (lipophilic) properties of small organic molecules using fragmental methods: an analysis of ALOGP and CLOGP methods. *J Phys Chem A* **102:**3762–3772.

Groves CE, Evans K, Dantzler WH, and Wright SH (1994) Peritubular organic cation transport in isolated rabbit proximal tubules. *Am J Physiol* **266:**F450–F458.

Karbach U, Kricke J, Meyer-Wentrup F, Gorboulev V, Volk C, Loffing-Cueni D, Kaissling B, Bachmann S, and Koepsell H (2000) Localization of organic cation transporters OCT1 and OCT2 in rat kidney. *Am J Physiol* **279:**F679–F687.

Koepsell H (1998) Organic cation transporters in intestine, kidney, liver and brain. *Annu Rev Physiol* **60:**243–266.

Malo C and Berteloot A (1991) Analysis of kinetic data in transport studies: new insights from kinetic studies of Na^+-D-glucose cotransport in human intestinal brush-border membrane vesicles using a fast sampling, rapid filtration apparatus. *J Membrane Biol* **122:**127–141.

Meyer-Wentrup F, Karbach U, Gorboulev V, Arndt P, and Koepsell H (1998) Membrane localization of the electrogenic cation transporter ROCT1 in rat liver. *Biochem Biophys Res Commun* **248:**673–678.

Nelsestuen GL and Martinez MB (1997) Steady state enzyme velocities that are independent of [enzyme]: an important behavior in many membrane and particle-bound states. *Biochemistry* **36:**9081–9086.

Pritchard JB and Miller DS (1993) Mechanisms mediating renal secretion of organic anions and cations. *Physiol Rev* **73:**765–796.

Ullrich KJ (1997) Renal transporters for organic anions and cations. Structural requirements for substrates. *J Membrane Biol* **158:**95–107.

Ullrich KJ (1999) Affinity of drugs to the different renal transporters for organic anions and organic cations. *Pharm Biotechnol* **12:**159–179.

Ullrich KJ, Papavassiliou F, David C, Rumrich G, and Fritzsch G (1991) Contraluminal transport of organic cations in the proximal tubule of the rat kidney. I. Kinetics of N1-methylnicotinamide and tetraethylammonium, influence of K+, HCO3-, pH; inhibition by aliphatic primary, secondary and tertiary amines and mono- and bisquaternary compounds. *Pflueg Arch Eur J Physiol* **419:**84–92.

Ullrich KJ, Rumrich G, and Fritzsch G (1992) Contraluminal transport of organic cations in the proximal tubule of the rat kidney. II. Specificity: anilines, phenylalkylamines (catecholamines), heterocyclic compounds (pyridines, quinolines, acridines). *Pflueg Arch Eur J Physiol* **420:**29–38.

van Montfoort JE, Muller M, Groothuis GM, Meijer DK, Koepsell H, and Meier PJ (2001) Comparison of "type I" and "type II" organic cation transport by organic cation transporters and organic anion-transporting polypeptides. *J Pharmacol Exp Ther* **298:**110–115.

Viswanadhan VN, Ghose AK, Revankar GR, and Robins RK (1989) atomic physicochemical parameters for three dimensional structure directed quantitative structure-activity relationships. 4. Additional parameters for hydrophobic and dispersive interactions and their application for an automated superposition of certain naturally occurring nucleoside antibiotics. *J Chem Inf Comput Sci* **29:**163–172.

Wong LT, Smyth DD, and Sitar DS (1990) Stereoselective inhibition of amantadine accumulation by quinine and quinidine in rat renal proximal tubules and cortical slices. *J Pharmacol Exp Ther* **255:**271–275.

Wright SH and Wunz TM (1999) Influence of substrate structure on substrate binding to the renal organic cation/H^+ exchanger. *Pflueg Arch Eur J Physiol* **437:**603–610.

Wright SH, Wunz TM, and Wunz TP (1995) Structure and interaction of inhibitors with the TEA/H^+ exchanger of rabbit renal brush border membranes. *Pflueg Arch Eur J Physiol* **429:**313–324.

Zhang L, Dresser MJ, Gray AT, Yost SC, Terashita S, and Giacomini KM (1997) Cloning and functional expression of a human liver organic cation transporter. *Mol Pharmacol* **51:**913–921.

Zhang L, Gorset W, Dresser MJ, and Giacomini KM (1999) The interaction of *N*-tetraalkylammonium compounds with a human organic cation transporter, HOCT1. *J Pharmacol Exp Ther* **288:**1192–1198.

Zhang L, Gorset W, Washington CB, Blaschke TF, Kroetz DL, and Giacomini KM (2000) Interactions of HIV protease inhibitors with a human organic cation transporter in a mammalian expression system. *Drug Metab Dispos* **28:**329–334.

Zhang L, Schaner ME, and Giacomini KM (1998) Functional characterization of an organic cation transporter (HOCT1) in a transiently transfected human cell line (HeLa). *J Pharmacol Exp Ther* **286:**354–361.

Address correspondence to: Stephen H. Wright, Department of Physiology, College of Medicine, University of Arizona, Tucson, AZ 85724. E-mail: shwright@u.arizona.edu